Aerodynamic force analysis in high Reynolds number flows by Lamb vector integration

Claudio Marongiu[1], Renato Tognaccini[2]
[1]*CIRA, Italian Center for Aerospace Research, Capua (CE), Italy*
E-mail: c.marongiu@cira.it

[2]*Dipartimento di Ingegneria Aerospaziale, Universita' Federico II, Napoli, Italy*
E-mail: rtogna@unina.it

Keywords: Aerodynamic force, Lamb vector, high Reynolds flows

The aerodynamic force experienced by a solid body and the physical interpretation of the processes involved in its genesis represents an issue of fundamental importance in the fluid dynamics. The *far field* formulations, alternative to the standard *near field* expression of the aerodynamic force, are introduced because they bring together several advantages in the physical understanding and technical applications. A recent *far field* theory clarifies the role of the Lamb vector in the generation of the aerodynamic force for an incompressible viscous flow. In the present paper this theory is reviewed and numerically applied for flows at high Reynolds numbers in steady and unsteady conditions. For these scopes, a straightforward extension to the analysis of flows governed by the Reynolds Averaged Navier Stokes equations has also been proposed. As applicative examples, the aerodynamic force (lift and drag) of a two dimensional airfoil under steady and unsteady conditions is computed by means of Lamb vector integrals.

1 Introduction

The aerodynamic force $\underline{\mathbf{F}}$, by means of the momentum balance equation, can be expressed in two alternative formulations, the *near field* and the *far field* one, as follows:

$$\underline{\mathbf{F}} = \underbrace{\int_{\partial B} (p\,\underline{\underline{\mathbf{I}}} - \underline{\underline{\tau}}) \cdot \underline{n} dS}_{Near field} = \underbrace{-\int_{\Sigma} (\rho\,\underline{\mathbf{u}}\,\underline{\mathbf{u}} + p\,\underline{\underline{\mathbf{I}}} - \underline{\underline{\tau}}) \cdot \underline{n} dS}_{Far field} \tag{1}$$

where ∂B is the surface of a solid body B and Σ is the external surface of a fixed control volume Ω, see figure 1(a). In equation (1), p is the pressure, $\underline{\underline{\mathbf{I}}}$ is the unit tensor, $\underline{\underline{\tau}}$ is the viscous stress tensor, $\underline{n}$ is the normal versor, positive when pointing outward, ρ is the flow density and $\underline{\mathbf{u}}$ is the velocity vector. The equation (1) is valid for a compressible steady and viscous flow. Even though the *far field* formulation is formally equivalent to the *near field* form, it is often used to address several specific issues of the Applied Aerodynamics.

In the experimental aerodynamics context, the need of using alternative approaches to the *near field* form appeared very quickly. The correlation of the profile drag component of an airfoil with the flow defect in the wake represented the first effective application of the *far field* form (Betz, 1925).

In principle, the Computational Fluid Dynamics (CFD) should not be touched by these aspects. The continuous growth of the computer power allows for aerodynamic analyses of more and more complex configurations. Nevertheless, this does not assure a reliable confidence on the calculated drag component, even if the solution is locally accurate, because of discretization error and artificial viscosity effects, (see van Dam (1999) for a comprehensive review). Among the various numerical

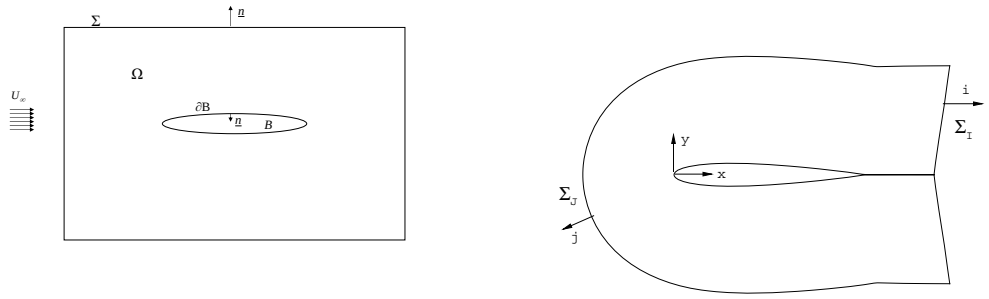

(a) (b)

Figure 1: (a) Schematic representation of the control volume Ω, the body surface ∂B and external surface Σ. (b) Specialization of the control volume Ω for an airfoil, the wake surface Σ_I and the outer surface Σ_J.

methodologies, it has also been shown how the *far field* formulation can aid in the identification of spurious numerical contributions associated with the prediction of the aerodynamic force, (Paparone & Tognaccini (2003), Destarac & van der Vooren (2004)).

The breakdown of the aerodynamic drag is another research branch in which the *far field* methods give a significant contribution. The possibility to recognize the specific components of the physical processes involved is of fundamental importance for the aerodynamic designers. Of particular interest is the identification of the induced drag component over a finite wing in case of a real flow.

However, the research on the prediction and breakdown of the aerodynamic force has been limited to the analysis of steady flows. The extension to unsteady flows necessarily increases the complexity of the formulation. Wu J. C. (1981) showed a correlation of the aerodynamic force to the first moment of the vorticity, applicable also to unsteady flows by supposing a fluid at rest at infinity in an unbounded domain. Panda & Zaman (1994) used such result in a wind tunnel facility by measuring the vorticity around an oscillating airfoil so showing the practical possibility to infer the unsteady aerodynamic force. Wu J.Z. & al. (2006), recently extended the Wu J.C.'s formulation to a more general case by removing some of the hypotheses underlying the previous theory of the 1981. In this theory, the Lamb vector $\underline{\boldsymbol{l}}$, defined as $\underline{\omega} \times \underline{\mathbf{u}}$ (where $\underline{\omega}$ is the vorticity and $\underline{\mathbf{u}}$ is the velocity), appears to be the key quantity in the generation of the aerodynamic force. Besides, Wu J.Z. & al. (2007) showed the first numerical applications of this theory to flows at low Reynolds number.

The aim of the present paper is to propose a specialization of Wu J.Z.'s theory for flows at high Reynolds number. For this purpose, flow solutions arising from the Euler equations and the Reynolds Averaged Navier Stokes (RANS) equations have been considered. In § 2 a brief recall of the theory proposed by Wu J.Z. with a formal extension for RANS solutions is reported. Applications to inviscid and viscous flow fields around a two dimensional airfoil in both steady and unsteady conditions are presented in § 3. Comparisons of the aerodynamic force computed between the *far field* technique and the classical wall integration method are shown to verify and validate the theory. In § 4, some concluding remarks are drawn.

2 Far field formulation of the aerodynamic force

Consider a solid body B immersed in a free stream flow U_∞. Let Σ be an external surface surrounding the solid body B, as sketched in figure 1(a). By specifying with Ω the flow domain, Wu

J.Z. provides the expression of the aerodynamic force $\underline{\mathbf{F}}$ through the sum of three contributions:

$$\underline{\mathbf{F}} = \underline{\mathbf{F}}_{I} + \underline{\mathbf{F}}_{II} + \underline{\mathbf{F}}_{III} \tag{2}$$

The contribution $\underline{\mathbf{F}}_{I}$ has two alternative and equivalent expressions, named *diffusion* $\underline{\mathbf{F}}_{I,d}$ and *advection* $\underline{\mathbf{F}}_{I,a}$ form respectively. They are:

$$\underline{\mathbf{F}}_{I,d} = -\int_{\Omega} \left(\underline{\mathbf{x}}' \times \mu \nabla^2 \underline{\omega} \right) dV \tag{3a}$$

$$\underline{\mathbf{F}}_{I,a} = -\int_{\Omega} \left(\underline{\mathbf{x}}' \times \rho \frac{\partial \underline{\omega}}{\partial t} \right) dV - \int_{\Omega} \rho \underline{\boldsymbol{l}} \, dV - \int_{\partial\Omega} \underline{\mathbf{x}}' \times (\underline{n} \times \rho \underline{\boldsymbol{l}}) \, dS \tag{3b}$$

where μ is the dynamic viscosity, $\underline{\mathbf{x}}' = \underline{\mathbf{x}} / (d-1)$, $\underline{\mathbf{x}}$ is the position vector and $d = 2, 3$ is the space dimension. The vortex force, namely, the volume integral of the Lamb vector, appears explicitly in equation (3b). The contribution $\underline{\mathbf{F}}_{II}$ is made up of surface integrals on Σ:

$$\underline{\mathbf{F}}_{II} = -\int_{\Sigma} \left(\underline{\mathbf{x}}' \times \left[\, \underline{n} \times \mu \, (\underline{\nabla} \times \underline{\omega}) \, \right] \right) dS + \int_{\Sigma} \mu \, (\underline{\omega} \times \underline{n}) \, dS \tag{3c}$$

The contribution $\underline{\mathbf{F}}_{III}$ is associated with the local solid body acceleration $\underline{\mathbf{a}}$, which is zero in case of a stationary motion.

$$\underline{\mathbf{F}}_{III} = \int_{\partial B} \underline{\mathbf{x}}' \times (\, \underline{n} \times \rho \, \underline{\mathbf{a}}) \, dS \tag{3d}$$

It is worth to note that in equation (3b) the surface integrals on $\partial\Omega$ in steady case may be reduced to Σ because $\underline{\mathbf{u}} \cdot \underline{n} = 0$ on ∂B. Moreover, for the unsteady case, this contribution can be embodied in (3d) as follows:

$$\underline{\mathbf{F}}_{III} = \int_{\partial B} \underline{\mathbf{x}} \times \left[\, \underline{n} \times \rho \, (\, \underline{\mathbf{a}} - \underline{\boldsymbol{l}}) \, \right] dS \tag{4}$$

Once a fluid dynamic field is provided, the theory of Wu, as formulated in equations (3), allows for computing the aerodynamic force in terms of vorticity $\underline{\omega}$ and Lamb vector $\underline{\boldsymbol{l}}$ fields. Applications of such results have been shown by Wu J.Z. & al. (2007) for circular cylinder flows at Reynolds $\sim 10^4$. However, it has been supposed that the fluid dynamic field is governed by the Navier Stokes equations in laminar flow regime. Therefore, further analyses are needed before applying such results to flow solutions at high Reynolds number.

2.1 Fully inviscid flows

In case of an inviscid but rotational flow, the dynamic viscosity $\mu = 0$. As a consequence, by equations (3), $\underline{\mathbf{F}}_{II}$ and $\underline{\mathbf{F}}_{I,d}$ are zero. From the equivalence of the *diffusion* and *advection* forms, we should also have $\underline{\mathbf{F}}_{I,a} = 0$. But this equivalence only subsists for viscous flows. In fact, by decomposing the vorticity into two components, one of which parallel to the velocity direction, $\underline{\omega} = \underline{\omega}_{\parallel} + \underline{\omega}_{\perp}$, it results a non zero Lamb vector field $\underline{\boldsymbol{l}}$ if the component $\underline{\omega}_{\perp} \neq 0$. The steady inviscid flow around an airfoil with a sharp trailing edge experiences a non zero aerodynamic force just due to a non zero $\underline{\omega}_{\perp}$. Such force can only be computed by the *advection* form (3b).

2.2 Laminar boundary layer flows

By specifying with ϕ_r the reference quantity of ϕ and with ϕ^* the corresponding non dimensional quantity, the non dimensional expressions of equations (3) are:

$$\underline{\mathbf{F}}^*_{I,\,d} = -\frac{1}{Re_r}\int_{\Omega^*}\left(\underline{\mathbf{x}}'^* \times \nabla^2\underline{\omega}^*\right) dV^* \tag{5a}$$

$$\underline{\mathbf{F}}^*_{I,\,a} = -\int_{\Omega^*}\left(\underline{\mathbf{x}}'^* \times \frac{\partial\underline{\omega}^*}{\partial t^*}\right) dV^* - \int_{\Omega^*}\underline{\boldsymbol{l}}^*\, dV^* - \int_{\partial\Omega^*}\underline{\mathbf{x}}'^* \times (\underline{n}\times\underline{\boldsymbol{l}}^*)\, dS^* \tag{5b}$$

$$\underline{\mathbf{F}}^*_{II} = -\frac{1}{Re_r}\int_{\Sigma^*}\left(\underline{\mathbf{x}}'^* \times [\underline{n}\times(\underline{\nabla}\times\underline{\omega}^*)]\right) dS^* + \frac{1}{Re_r}\int_{\Sigma^*}(\underline{\omega}^*\times\underline{n})\, dS^* \tag{5c}$$

$$\underline{\mathbf{F}}^*_{III} = \int_{\partial B^*}\underline{\mathbf{x}}'^* \times (\underline{n}\times\underline{\mathbf{a}}^*)\, dS^* \tag{5d}$$

where $Re_r = \rho_r U_r L_r/\mu$ is the Reynolds number and $\underline{\mathbf{F}} = \rho_r U_r^2 L_r^2\,\underline{\mathbf{F}}^*$. Only $\underline{\mathbf{F}}^*_{I,\,d}$ and $\underline{\mathbf{F}}^*_{II}$ explicitly depend on the Reynolds number. In case of a laminar boundary layer flow ($Re \gg 1$), the classical analysis of the orders of magnitude allows for neglecting the integral $\underline{\mathbf{F}}^*_{II}$ and computing the aerodynamic force by using only the contributions $\underline{\mathbf{F}}^*_{I,\,a}$ or $\underline{\mathbf{F}}^*_{I,\,d}$.

2.3 Turbulent boundary layer flows

In case of turbulent flows, the numerical methods most widely used are based on space filtered or time averaged Navier Stokes equations, commonly referred as LES (Large Eddy Simulation) or RANS (Reynolds Averaged Navier Stokes) methods. In both cases, the filter process introduces an extra term in the momentum equation having the form of a second order tensor $\underline{\underline{\tau}}^t$, (Pope , 2000). By referring hereafter to the RANS equations and by indicating with $\langle\phi\rangle$ the averaged value of ϕ, equations (5) have to be transformed according to the average procedure. However, it is possible to verify that while the Reynolds averaged *advection* form is obtainable by substituting the corresponding averaged quantities in the integrand function, this does not occurr for the *diffusion* form, where new terms associated with $\underline{\underline{\tau}}^t$ appear. However, some simplifications are allowed in the hypothesys of turbulent boundary layer. According to Pope (2000), in the boundary layer theory, only the derivatives of the shear stress components $\langle u'v'\rangle$ with respect to the wall normal distance y have the same order of magnitude of the mean quantities. Thus, within this approximation the integral (5c) reduces to:

$$\langle\,\underline{\mathbf{F}}_{II}\,\rangle \approx \int_{\Sigma}\frac{\partial\,\langle u'v'\rangle}{\partial\,y}\,n_y\left(y\,\underline{i} - x\,\underline{j}\right) dS \tag{6}$$

where $\underline{i}$ and $\underline{j}$ are unit vectors, and n_y is the wall normal component of $\underline{n}$. It is worth noting that this contribution is zero on Σ when $\underline{n} = \underline{i}$, but in the general case it can not be neglected as in laminar boundary layer flows.

3 Applications

Although the *diffusion* and *advection* form are equivalent, the latter shows several advantages in the application context. At first, the *diffusion* form requires the calculation of the third spatial derivative of the velocity field, cumbersome if the spatial resolution is not sufficient. On the contrary, first order derivatives are only required for the *advection* form. Another problem is that, in case of

turbulent flows, the *diffusion* form $\langle \underline{\mathbf{F}}_{I,d} \rangle$ involves the Reynolds stress tensor $\underline{\underline{\tau}}^t$. In addition, it can not be applied in case of inviscid flows.

In figure 1(b) it is proposed a selection of the integration domain Ω based on a typical computational grid used for CFD calculations around two dimensional airfoils. The external surface Σ is divided into two parts, Σ_I and Σ_J, obtained by fixing a grid line at an index i and j respectively. By specializing the integrals (3) and the body surface contribution (4) in an orthogonal cartesian reference system Oxy, with the x axis parallel to U_∞, we have:

$$C_l = -2 \int_\Omega \left(l_y - x \frac{\partial \omega}{\partial t}\right) dV + 2 \int_\Sigma x\, \omega\, (\underline{\mathbf{u}} \cdot \underline{n})\, dS - 2 \int_{\partial B} x\, a_B\, dS \tag{7a}$$

$$C_d = -2 \int_\Omega \left(l_x + y \frac{\partial \omega}{\partial t}\right) dV - 2 \int_\Sigma y\, \omega\, (\underline{\mathbf{u}} \cdot \underline{n}) dS + 2 \int_{\partial B} y\, a_B\, dS \tag{7b}$$

where $a_B = |\underline{n} \times (\underline{\mathbf{a}} - \underline{\boldsymbol{l}})|$. It is straightforward to see that $\underline{\mathbf{a}} - \underline{\boldsymbol{l}}$ on ∂B is always normal to the direction joining the rotation centre and the surface point together. As a consequence, for thin oscillating airfoils a_B results negligible.

In the following, such results will be applied to numerical solutions of two dimensional flows around a NACA0012 airfoil at high Reynolds number obtained from a standard CFD code for aerodynamics applications (Jameson & al. , 1981). The C-type computational grid used for the inviscid flow computations has 448×112 cells in stream wise and normal wise directions respectively. For turbulent computations, the grid used has 768×200 cells. In both the cases, the external boundary is located at about 30 chord units from the airfoil surface. Some tests with a domain of about 100 chords have also been performed. The turbulent calculations are performed through a RANS approach with a $\kappa - \omega$ turbulence model (Kok (2000)). The integrals are numerically computed using the cell centered data of the flow solver output. The data are considered as averages over the cell volume, which is consistent with the discretization of the flow equations.

3.1 Steady and inviscid flow around airfoils

The lift on an airfoil immersed in an inviscid and steady flow field can be computed using equation (7a). Nevertheless, a numerical solution of the steady Euler equations around an airfoil does not provide any vorticity in the field and, as a consequence, the integrals of the Lamb vector should not be able to provide the correct lift value. However, equation (7a) can be applied in a fully inviscid flow by considering the Euler solution as a limit of a Navier Stokes solution for $Re \to \infty$. Assuming a zero velocity at the wall, a vorticity layer extending for $\varepsilon/2$ is created.

$$\underline{\omega}_{\varepsilon/4} = \frac{2\, \underline{\mathbf{u}}_1}{\varepsilon} \times \underline{n} \tag{8}$$

where ε is the normal spacing of the first cell near the solid wall, and $\underline{\mathbf{u}}_1$ is the corresponding flow velocity. As a conseqnence, the Lamb vector is:

$$\underline{\boldsymbol{l}}_{\varepsilon/4} = \underline{\omega}_{\varepsilon/4} \times \underline{\mathbf{u}}_{\varepsilon/4} = \left(\frac{2\, \underline{\mathbf{u}}_1}{\varepsilon} \times \underline{n}\right) \times \underline{\mathbf{u}}_{\varepsilon/4} \tag{9}$$

where $\underline{\mathbf{u}}_{\varepsilon/4} = 0.5\, \underline{\mathbf{u}}_1$ is the velocity at $r = \varepsilon/4$. Thus, by computing the Lamb vector integral in a volume Ω surrounding the solid body, having a thickness $\varepsilon/2$ in the normal direction it is possible

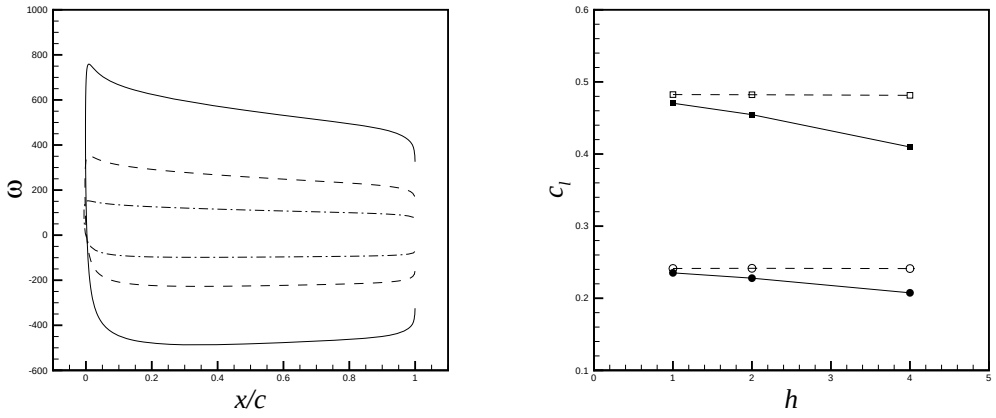

(a) (b)

Figure 2: NACA0012 airfoil, fully inviscid flow solutions. (a) Wall vorticity computed using equation (9). —, $h = 1$; $--$, $h = 2$; $- \cdot -$, $h = 4$. (b) Lift coefficients: open symbols refer to the *near field* method, full symbols to the *far field* method. Circle, $\alpha = 2°$; square, $\alpha = 4°$.

to show that such integral supplies the standard *near field* expression of the aerodynamic force in an inviscid steady flow. This result has been verified on the numerical inviscid solution around the NACA0012 airfoil at $\alpha = 2°$ and $\alpha = 4°$. In figure 2(a) the vorticity at the wall computed by using equation (9) is plotted versus the airfoil chord for the solution at $\alpha = 4\,°$, for different mesh size. As it can be observed, the vorticity intensity grows as grid spacing ratio h [1] decreases. In figure 2(b), the lift coefficients computed by refining the grid are reported. These values are computed with both the *near field* formula and equation (7a). The Lamb vector integral converges towards the *near field* result as $h \to 0$.

3.2 Inviscid and unsteady flow around airfoils

An inviscid flow around an oscillating airfoil is characterized by a release of *free* vorticity $\underline{\omega}^f$ in the flow field. This vorticity is responsible for the time delay between the aerodynamic force and the airfoil angular position, and it is superimposed to the *bound* vorticity $\underline{\omega}^b$ associated with the airfoil surface. In this section it will be shown how the use of Lamb vector integrals allows for a decomposition of the aerodynamic force of kind $C_l = C_l^f + C_l^b$, where C_l^f and C_l^b are the contributions associated with $\underline{\omega}^f$ and $\underline{\omega}^b$ respectively.

In fact, while the total lift coefficient is obtainable by equation (7a) considering the Lamb vector $\underline{\boldsymbol{l}}_{\varepsilon/4}$ as done in the steady case, the contribution C_l^f is given by integrating the vorticity field shed in the wake, namely, by the surface integral on Σ_I, located just downstream the airfoil.

The numerical solution of the Euler equations around the NACA0012 airfoil has been considered by imposing a pitching periodic motion with the rotation axis at $(0.25, 0)$. The angle of attack law is $\alpha = 7.5° \sin(2kt)$, where $k = 0.05$ is the reduced frequency. The analytical solution provided by Theodorsen (1935) for a moving flat plate has also been reported as a reference. The integration domain Ω has been selected by locating the surface Σ_I just downstream the trailing edge of the

[1] $h = \sqrt{N_f/N_c}$, N_f and N_c are the cell numbers of the fine and coarse grids.

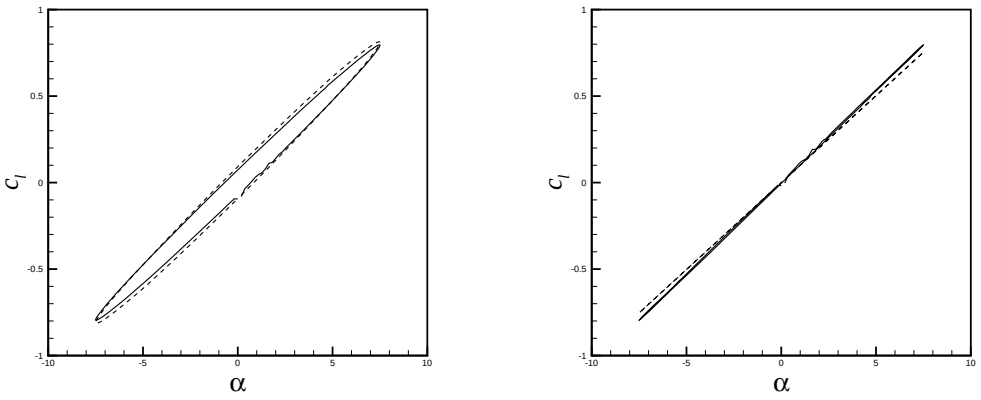

Figure 3: NACA0012, fully inviscid unsteady flow solution, $\alpha = 7.5° \sin(2kt)$, $k = 0.05$. Comparisons of the hysteresis curves of lift coefficient. (a) —, *far field* ; $--$, *near field.* (b) —, *bound* vorticity contribution; $--$, real part of Theodorsen solution.

airfoil, and the surface Σ_J near the outer boundary. In figure 3(a), a comparison between the lift hysteresis curve computed through equation (7a) and the *near field* method is shown. The curves are plotted as function of the instantaneous flow incidence α. Equation (7a) provides a good agreement with respect to the wall integrated data. In figure 3(b), the effects of the *bound* vorticity $\underline{\omega}^b$ are detected by plotting the real part of the Theodorsen solution and the contribution associated with the surface Σ_I. As expected, such contributions provide a curve practically in phase with respect to the instantaneous angular position. The real part of Theodorsen's solution shows a slightly different slope due to the effects of the finite thickness of the airfoil. As pointed out before, the contribution of the body surface integral has a negligible effect on the total lift coefficient.

3.3 Turbulent steady flow around airfoils

The *far field* computation of the aerodynamic coefficients has been applied to a steady turbulent flow around a two dimensional airfoil. Three Reynolds numbers have been investigated, $Re = 10^6$, 5×10^6, and 10^7 at angles of attack $0° \leq \alpha \leq 6°$. The aerodynamic coefficients have been calculated by varying the location of the surfaces Σ_I and Σ_J. Furthermore, each contribution has been normalized by the corresponding *near field* coefficient in a such way:

$$(C_l)^* = \frac{(C_l)_{Farfield}}{(C_l)_{Nearfield}} \quad ; \quad (C_d)^* = \frac{(C_d)_{Farfield}}{(C_d)_{Nearfield}}$$

where the superscript $*$ specifies the normalized coefficient. In the following the discussion for the Σ_I and Σ_J dependency is presented separately.

- *Influence of Σ_I position*
  In figure 4(a) the effects on the aerodynamic force computation by moving the surface Σ_I from the airfoil trailing edge ($x/c = 1$) to the external boundary ($x/c = 30$) is visible. The surface Σ_J is kept fixed at a distance L of about 30 chord units from the airfoil. For shortness, only the lift coefficient is examined. Although different α and Reynolds numbers flow solutions

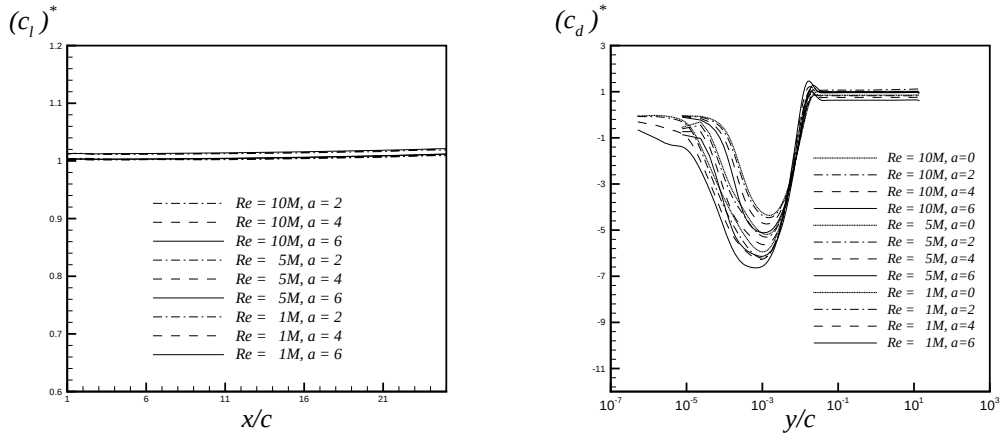

(a) (b)

Figure 4: NACA0012 airfoil, turbulent flow solutions at Reynolds numbers 10^6, $5 \cdot 10^6$ and 10^7. Angles of attack $\alpha = 2°$, $4°$ and $6°$. Normalized aerodynamic coefficients. (a) Effect of the Σ_I position on $(C_l)^*$. (b) Effect of the Σ_J position on $(C_d)^*$.

are reported, no significant dependency upon these parameters is visible. The $(C_l)^*$ is ≈ 1 within an approximation of 2% for all x although the computational mesh is quite coarse near the external boundary.

- *Influence of Σ_J position*
  In this case, the surface Σ_I is kept fixed just after the trailing edge airfoil, while the surface Σ_J is moved along the wall normal direction. The discussion is presented only for the drag coefficient. In figure 4(b), the $(C_d)^*$ is plotted as function of y, taken along the grid line of the Σ_I location. The logarithmic scale for the wall normal direction has been used to highlight the viscous region. It is shown that the integrals converge toward the *near field* values for y greater than the boundary layer thickness. Once the convergence is achieved, a very small dependency is visible upon α and the Reynolds number. In the boundary layer large overshoots are visible because of the neglected terms associated with the turbulent shear stress components as stated in § 2.3.

3.4 Turbulent unsteady flow around airfoils

Finally, the *far field* integrals (7) are applied to the analysis of an oscillating airfoil in turbulent flow conditions. The oscillating motion has been imposed through a sinusoidal variation of the angle of attack $\alpha = 7.5° \sin(2kt)$, with a reduced frequency $k = 0.05$ and Reynolds number $Re = 1.35 \cdot 10^5$. The integration domain Ω has been fixed with the surface Σ_I just downstream the airfoil trailing edge, and the surface Σ_J outside of the turbulent boundary layer. In figure 5(a) the hysteresis curve of the lift and drag coefficients is reported as function of the instantaneous incidence for both the *near field* and *far field* formulations. A very good agreement has been achieved. By using equations (7a) and (7b) several decompositions of the aerodynamic force are possible. In particular, following the unsteady inviscid flow analysis, the *free* vorticity $\underline{\omega}^f$ shed in the wake can be detected through the surface integral on Σ_I. For difference, the effect of the *bound* vorticity, reported in figure 5(b), is obtained by eliminating the Σ_I contribution. As in the fully inviscid case,

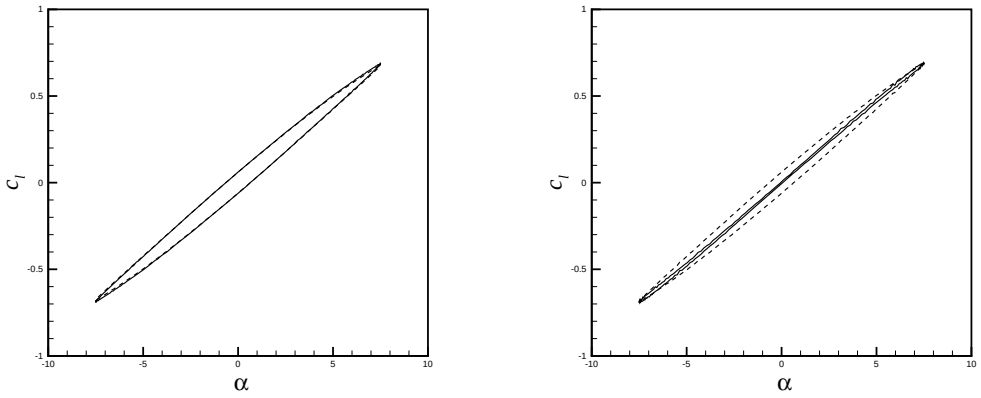

Figure 5: NACA0012 airfoil, unsteady turbulent flow solution at Reynolds number $Re = 1.35 \cdot 10^5$, $\alpha = 7.5^\circ \sin(2kt)$, $k = 0.05$. Comparison of the aerodynamic coefficients. —, *far field*; $--$, *near field* (a) Lift coefficient. (b) Lift coefficient associated with the *bound* vorticity.

this last one results to be practically in phase with the airfoil angular position α. The same kind of the decomposition has been applied to the drag coefficient but for shortness it has not reported here.

4 Conclusions

An incompressible *far field* analysis of the aerodynamic force on a two dimensional airfoil has been conducted by computing integrals of Lamb vector field. The theory on which such analysis is founded, was initially developed for viscous flows. In the present work it has been extendend and applied to various flow typologies characterized by high Reynolds numbers. For turbulent flows the theory has been made suitable for the Reynolds Averaged Navier Stokes equations. Four kind of applications have been shown.

In case of fully inviscid and steady flows, a method to introduce a proper Lamb vector field near the solid walls has been proposed by interpreting the Euler flow as limit of a Navier Stokes solution. In this way the correct aerodynamic force can also be obtained from a numerical solution of the Euler equations.

This result has also been extended to an unsteady inviscid flow solution around an oscillating airfoil. The contribution of the *free* vorticity shed in the wake has been detected by the Lamb vector integrals and compared with the analytical results provided by Theodorsen for an oscillating flat plate. The *bound* vorticity contribution has also been identified as the component of the aerodynamic force in phase with the instantaneous angular position of the airfoil.

The extension of the theory to turbulent flows has permitted to deal with numerical solutions governed by the Reynolds Averaged Navier Stokes equations. It has been shown that in case of laminar boundary layer approximation, some contributions of the complete expression of the aerodynamic force are negligible. In case of turbulent boundary layer, the same analysis remarks the importance of a term associated with the turbulent stress tensor. However, it has been shown that through a proper choice of the external surface orientation this contribution does not need to be computed.

The effect of the integration domain has been investigated at different Reynolds numbers and angles of attack.

From a numerical point of view, the most accurate values of the aerodynamic force have been obtained with an integration domain that intersects the wake just downstream the airfoil trailing edge and that contains the whole boundary layer region. A certain dependency upon the outer boundary conditions has been noted.

Finally, the case of an unsteady and turbulent flow field around an oscillating airfoil has been discussed. Analogously to the fully inviscid case, the effect of the *bound* vorticity has also been recognized as the contribution in phase with the instantaneous angular position of the airfoil.

References

BETZ, A. 1925 *A Method for the Direct Determination of Profile Drag*. ZFM, **16**.

VAN DAM, C. P. 1999 Recent Experience with Different Methods of Drag Prediction. *Progress in Aerospace Sciences*, **35**, 751–798.

DESTARAC, D., VAN DER VOOREN, J. 2004 Drag-thrust analysis of jet-propelled transonic transport aircraft, definition of physical drag components. *Aerospace Science and Technology*, **8**, 545–556.

JAMESON, A., SCHMIDT, W. AND TURKEL, E. 1981 Numerical Solutions of the Euler Equations by Finite Volume Methods Using Runge-Kutta Time Stepping Schemes. *AIAA Paper* 1981-1259.

KOK, J. 2000 Resolving the Dependence on Free-Stream Values for the κ-ω Turbulence Model. *AIAA Journal*, **38**, 7, 1292–1295.

PANDA, J., ZAMAN, K. B. M. Q. 1994 Experimental investigation of the flow field of an oscillating airfoil and estimation of lift from wake surveys. *J. of Fluid Mech.*, **265**, 65–95.

PAPARONE, L. & TOGNACCINI, R. 2003 Computational Fluid Dynamics-Based Drag Prediction and Decomposition. *AIAA Journal* **41**, 9.

POPE S. B. 2000 *Turbulent flows* Cambridge University Press.

THEODORSEN, T. 1935 General theory of aerodynamic instability and the mechanism of flutter. *NACA-Report*, 496.

TOGNACCINI, R. 2003 Methods for drag decomposition, Thrust-drag bookkeeping from CFD calculations. *VKI Lecture Series 2003-02, CFD-Based*.

WU, J. C. 1981 Theory for Aerodynamic Force and Moment in Viscous Flows. *AIAA Journal*, **19**, 4.

WU, J.-Z., MA H. -Y. & ZHOU M. -D. 2006 *Vorticity and Vortex Dynamics*. Springer.

WU, J.-Z., LU X.-Y., ZHUANG L.-X 2007 Integral force acting on a body due to local flow structures *J. of Fluid Mech.*, **576**, 265–286.